Linear CO-Bridged, Dinuclear Tantalum Siloxycarbyne Complexes

Raymond N. Vrtis, Simon G. Bott, and Stephen J. Lippard*

Department of Chemistry, Massachusetts Institute of Technology, Cambridge, Massachusetts 02139

Received June 17, 1991

Reaction of $Na[Ta(CO)_2(dmpe)_2]$ with 1 equiv of trimethylsilyl chloride initially yields the siloxycarbyne species, $[Ta(\equiv COSiMe_3)(CO)(dmpe)_2]$, which converts in the presence of NaCl to the CO-bridged complex, $[(dmpe)_2(CO)TaCOTa(Me_3SiOCCOSiMe_3)(dmpe)_2]$. The structure of the *tert*-butyldimethylsilyl analogue was determined by a single-crystal X-ray diffraction study. The carbonyl bridge in $[(dmpe)_2(CO)TaCO-Ta(t\text{-}BuMe_2SiOCCOSiMe_2\text{-}t\text{-}Bu)(dmpe)_2]$ (**3b**) is nearly linear, the Ta–C–O and C–O–Ta angles being 169 and 166°, respectively. The bond distances in the Ta=C=O=Ta bridged unit are intermediate between that found in $[Ta(\equiv COSi(i\text{-}Pr)_3)(CO)(dmpe)_2]$ and other linear carbonyl-bridged species. This bond delocalization is reflected in the unusually low infrared stretching frequency, 1462 cm^{-1}, associated with the bridging Ta=C=O=Ta unit. An analogous CO-bridged dimetallic complex, $[(dmpe)_2(CO)-TaCOZrCp^*_2Cl]$ (**4**), was prepared by the reaction of $Na[Ta(CO)_2(dmpe)_2]$ with 1 equiv of $Cp^*_2ZrCl_2$ and also structurally characterized. A mechanism for the formation of these CO-bridged species is proposed. Both complexes react with 2 equiv of trimethylsilyl chloride to yield the known coupled product $[Ta-(Me_3SiOCCOSiMe_3)(dmpe)_2Cl]$. Such CO-bridged species are not required as an intermediate in the mechanism for the reductive coupling of carbon monoxide in $[Ta(CO)_2(dmpe)_2Cl]$ complexes, however. Crystal data: compound **3b** monoclinic, $P2_1/c$, a = 17.885 (8) Å, b = 21.041 (9) Å, c = 17.544 (5) Å, β = 114.74 (3)°, Z = 4; compound **4** triclinic, $P\bar{1}$, a = 12.288 (2) Å, b = 17.851 (2) Å, c = 9.687 (2) Å, α = 90.67 (1)°, β = 101.54 (1)°, γ = 80.46 (1)°, Z = 2.

Introduction

The activation of carbon monoxide in a manner that favors its conversion into useful organic products is a current objective in our laboratory.[1] One step toward achieving this goal would be the synthesis of compounds having a carbon monoxide molecule bound to two metal atoms in either a μ-η^1,η^2-CO (I) or μ-η^1,η^1-CO (II) fashion,

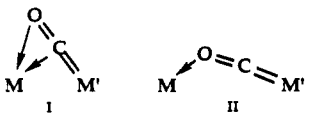

as shown. Binding of CO in such a fashion decreases the C–O bond strength, as evidenced by a significant lowering of the CO stretching frequency, and increases the C–O bond length, which should lead to increased reactivity. While there are numerous examples of such μ-isocarbonyl metal complexes in the literature,[2] their reaction chemistry has not been extensively explored. One early manifestation of the concept that positioning a carbonyl ligand between two metal centers might increase its reactivity is the discovery that two terminal carbonyl ligands within a diiron complex can be reductively coupled with concomitant binding to a zirconium center, as shown in eq 1.[3] This reaction exemplifies the synthetic potential of activating such a bridging carbonyl group.

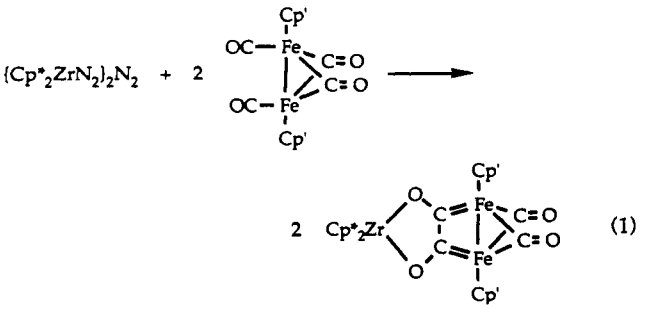

(1)

While the mechanism of reductive coupling of two carbonyl ligands in the compound $[Ta(CO)_2(dmpe)_2Cl]$ (**1**) was investigated, trialkylsiloxycarbyne species $[Ta-(\equiv COSiR_3)(CO)(dmpe)_2]$ (**2**)[4,5] were identified as key intermediates, eq 2. During the course of this work, a novel

$$[Ta(CO)_2(dmpe)_2Cl] \xrightarrow[(2)\ R_3SiCl]{(1)\ 40\%\ Na/Hg} \underset{\mathbf{1}}{} [Ta(\equiv COSiR_3)(CO)(dmpe)_2] \xrightarrow{R_3SiCl} \underset{\mathbf{2}}{} [Ta(R_3SiOC\equiv COSiR_3)(dmpe)_2Cl] \quad (2)$$

molecule, resulting from the formal dimerization of two trialkylsiloxycarbyne species, was obtained. This complex, $[(dmpe)_2(CO)TaCOTa(t\text{-}BuMe_2SiOCCOSiMe_2\text{-}t\text{-}Bu)-(dmpe)_2]$ (**3b**), was structurally characterized as a dinuclear tantalum complex containing a nearly linear bridging CO group. These results, as well as the formation and structural characterization of a related, linear CO-bridged heterodimetallic complex $[(dmpe)_2(CO)TaCOZrCp^*_2Cl]$ (**4**), obtained by reaction of $Cp^*_2ZrCl_2$ with $Na[Ta(CO)_2-(dmpe)_2]$ (**5**), are reported in the present article. The reactions of these complexes to afford reductively coupled carbonyl products are also described.

Experimental Section

Materials and Spectral Measurements. All reactions and manipulations were carried out either in a nitrogen-filled Vacuum Atmospheres drybox or under argon by using standard Schlenk line techniques. Solvents were distilled under nitrogen from sodium benzophenone ketyl and stored over 3-Å molecular sieves. Deuterated benzene was dried by passage through a column of alumina and stored over 3-Å molecular sieves. $[Ta(CO)_2-(dmpe)_2Cl]$ (**1**) was synthesized by using a modified literature procedure.[6,7] Sodium amalgam (40%) was prepared by a literature method.[8] Chlorotrimethylsilane (Me_3SiCl, Petrarch),

(1) Vrtis, R. N.; Lippard, S. J. *Isr. J. Chem.* **1990**, *30*, 331.
(2) Horwitz, C. P.; Shriver, D. F. *Adv. Organomet. Chem.* **1984**, *23*, 219.
(3) Berry, D. H.; Bercaw, J. E.; Jircitano, A. J.; Mertes, K. B. *J. Am. Chem. Soc.* **1982**, *104*, 4712.
(4) Vrtis, R. N.; Rao, C. P.; Warner, S.; Lippard, S. J. *J. Am. Chem. Soc.* **1988**, *110*, 2669.
(5) Vrtis, R. N.; Liu, S.; Rao, C. P.; Bott, S. G.; Lippard, S. J. *Organometallics* **1991**, *10*, 275.
(6) Datta, S.; Wreford, S. S. *Inorg. Chem.* **1977**, *16*, 1134.
(7) Bianconi, P. A. Ph.D. Thesis, Massachusetts Institute of Technology, 1986.

0276-7333/92/2311-0270$03.00/0

chloro-*tert*-butyldimethylsilane (*t*-BuMe$_2$SiCl, Petrarch), and bis(pentamethylcyclopentadienyl)zirconium dichloride (Cp*$_2$ZrCl$_2$, Strem) were obtained from commercial sources and used without further purification. ^{1}H, ^{31}P{^{1}H}, and ^{13}C{^{1}H} NMR spectra were recorded on a Varian XL-300 instrument. Proton chemical shifts were referenced to residual solvent protons and ^{31}P{^{1}H} chemical shifts to external 85% phosphoric acid. Infrared spectra were measured on a Mattson Cygnus 100 FTIR spectrometer. Elemental analyses were performed by Desert Analysis, Tucson, AZ.

Preparation of [(dmpe)$_2$(CO)TaCOTa(Me$_3$SiOCCOSiMe$_3$)(dmpe)$_2$] (3a). A mixture of 0.090 g (0.158 mmol) of [Ta(CO)$_2$(dmpe)$_2$Cl] (1), >100-fold excess 40% sodium amalgam, and 10 mL of THF was stirred in a 25-mL flask for 5 h, during which time the color changed from orange to red-brown. After filtration, 20 μL (0.158 mmol) of Me$_3$SiCl was added to the solution, at which time the color changed from red-brown to plum-red. The THF was removed in vacuo, and the residue was dissolved in a minimal amount of pentane which, upon cooling to −30 °F for 24 h, yielded 0.042 g (44%) of [(dmpe)$_2$(CO)TaCOTa(Me$_3$SiOCCOSiMe$_3$)(dmpe)$_2$] (**3a**) as dark red plates. Spectroscopic data: FTIR (KBr pellet) 2959 (m), 2895 (s), 2812 (w), 1747 (s, ν_{CO}; shifts to 1707 upon use of ^{13}C-enriched CO in 1), 1572 (m, ν_{CO} or ν_{CC}; shifts to 1517 upon use of 90% ^{13}CO-enriched 1), 1462 (s, $\nu_{\mu\text{-}CO}$; shifts to 1430 upon use of ^{13}C-enriched CO), 1412 (s), 1290 (w), 1279 (w), 1257 (m), 1247 (m), 1129 (m), 1028 (m), 928 (s), 835 (s), 781 (m), 733 (m), 701 (m), 676 (m), 625 (s) cm^{-1}; ^{1}H NMR (C$_6$D$_6$, 300 MHz) δ 1.90–1.72 (br m, 4 H, PCH$_2$), 1.69 (br m, 12 H, PCH$_3$), 1.63 (d, 3 H, PCH$_3$, J_{PH} = 6 Hz), 1.62 (d, 3 H, PCH$_3$, J_{PH} = 6 Hz), 1.60 (d, 3 H, PCH$_3$, J_{PH} = 5.6 Hz), 1.54 (d, 3 H, PCH$_3$, J_{PH} = 5.6 Hz), 1.52 (d, 3 H, PCH$_3$, J_{PH} = 4 Hz), 1.51 (d, 3 H, PCH$_3$, J_{PH} = 2.8 Hz), 1.49 (d, 3 H, PCH$_3$, J_{PH} = 4 Hz), 1.48 (d, 3 H, PCH$_3$, J_{PH} = 2.8 Hz), 1.39 (d, 3 H, PCH$_3$, J_{PH} = 6 Hz), 1.37 (d, 3 H, PCH$_3$, J_{PH} = 5.2 Hz), 1.02 (d, 3 H, PCH$_3$, J_{PH} = 2 Hz), 0.78 (d, 3 H, PCH$_3$, J_{PH} = 2.8 Hz), 0.23 (s, 18 H, SiCH$_3$) ppm (12 methylene protons are unaccounted for because of broadening due to fluctionality and/or overlapping methyl proton resonances); ^{31}P{^{1}H} NMR (121 MHz, C$_6$D$_6$) δ 30.4, 30.1, 21.7, 19.8, 9.1, 1.5 ppm; ^{13}C{^{1}H} NMR (75 MHz, C$_6$D$_6$) δ 257.2 (s), 247.6 (s), 210.2 (quintet, $^2J_{CP}$ = 17 Hz). Anal. Calcd for C$_{34}$H$_{82}$O$_4$P$_8$Si$_2$Ta$_2$: C, 33.45; H, 6.77. Found: C, 32.99; H, 6.92.

Preparation of [(dmpe)$_2$(CO)TaCOTa(*t*-BuMe$_2$SiOCCOSiMe$_2$-*t*-Bu)(dmpe)$_2$] (3b). A mixture of 0.100 g (0.174 mmol) of [Ta(CO)$_2$(dmpe)$_2$Cl] (1), >100-fold excess 40% sodium amalgam, and 8 mL of THF was stirred in a 25-mL flask for 4 h, during which time the color changed from orange to red-brown. After filtration, 0.027 g (0.176 mmol) of *t*-BuMe$_2$SiCl was added to the solution, the color of which changed immediately from red-brown to plum-red. The THF was removed in vacuo and the residue was dissolved in a minimal amount of pentane which, upon cooling to −30 °F for 24 h, yielded dark red crystals of [(dmpe)$_2$(CO)TaCOTa(*t*-BuMe$_2$SiOCCOSiMe$_2$-*t*-Bu)(dmpe)$_2$] (**3b**). Spectroscopic data: ^{31}P{^{1}H} NMR (121 MHz, C$_6$D$_6$) δ 27.6 (2 P), 27.1 (2 P), 22.3 (1 P), 20.4 (1 P), 9.8 (1 P), 1.2 (1 P) ppm. Solutions from which **3b** was crystallized also contained ^{31}P resonances at 25.3, 24.5, 11.9, and 0.1 ppm, indicative of the presence of the mononuclear carbyne complex **2**. ^{13}C{^{1}H} NMR (75 MHz, C$_6$D$_6$) for 90% ^{13}CO-enriched material: δ 257.1, 248.5, 215.9 (quintet, J_{PC} = 12 Hz) ppm. The mononuclear carbyne complex present in solutions of **3b** has resonances at 252.3 and 244.0 ppm.

Reaction of [(dmpe)$_2$(CO)TaCOTa(Me$_3$SiOCCOSiMe$_3$)(dmpe)$_2$] (3a) with 1 Equiv of Sodium Iodide. To a solution of 0.032 g (0.026 mmol) of [(dmpe)$_2$(CO)TaCOTa(Me$_3$SiOCCOSiMe$_3$)(dmpe)$_2$] (**3a**) dissolved in THF-*d*$_8$ in an NMR tube was added 0.004 g (0.027 mmol) of NaI. After this mixture was allowed to react for 2 days at room temperature, the ^{31}P{^{1}H} NMR spectrum of this reaction mixture revealed three peaks at 22.6 and 8.0 and at 15.8 ppm, attributed to equal amounts of Na[Ta(CO)$_2$(dmpe)$_2$] and [Ta(Me$_3$SiOCCOSiMe$_3$)(dmpe)$_2$I], respectively, together with a peak at −48 ppm corresponding to free dmpe.

Reaction of [(dmpe)$_2$(CO)TaCOTa(Me$_3$SiOCCOSiMe$_3$)(dmpe)$_2$] (3a) with 2 Equiv of Trimethylsilyl Chloride. To a solution of 0.066 g (0.054 mmol) of [(dmpe)$_2$(CO)TaCOTa(Me$_3$SiOCCOSiMe$_3$)(dmpe)$_2$] (**3a**) in 5 mL of THF was added 14 μL (0.110 mmol) of Me$_3$SiCl. The reaction mixture was then stirred for 10 h, during which time the color of the solution changed from plum red to green. The ^{31}P{^{1}H} NMR spectrum of this reaction mixture revealed only one peak at 25 ppm, indicating clean formation only of [Ta(Me$_3$SiOCCOSiMe$_3$)(dmpe)$_2$Cl].

Preparation of [(dmpe)$_2$(CO)TaCOZrCp*$_2$Cl] (4). A mixture of 0.075 g (0.130 mmol) of [Ta(CO)$_2$(dmpe)$_2$Cl] (1), excess 40% sodium amalgam, and 8 mL of THF was stirred in a flask for 5 h, during which time the color changed from orange to red-brown. After filtration, 0.058 g (0.134 mmol) of Cp*$_2$ZrCl$_2$ was added to the solution, at which time there was a rapid color change from red-brown to deep violet. The THF was removed in vacuo, and the deep violet product was extracted into 20 mL of pentane which, upon cooling to −30 °F for 24 h, yielded 0.060 g (49.2%) of crystalline [(dmpe)$_2$(CO)TaCOZrCp*$_2$Cl] (**4**). Spectroscopic data: FTIR (KBr pellet) 2990 (w), 2902 (m), 2865 (w), 1732 (s, ν_{CO}), 1416 (m, $\nu_{\mu\text{-}CO}$), 1380 (m), 1285 (m), 1120 (w), 928 (m), 883 (w), 685 (w), 636 (w) cm^{-1}; ^{1}H NMR (300 MHz, C$_6$D$_6$) δ 2.06 (s, 15 H, CpCH$_3$), 2.05 (s, 15 H, CpCH$_3$), 1.87 (d, 3 H, PCH$_3$, J_{PH} = 6.8 Hz), 1.84 (d, 3 H, PCH$_3$, J_{PH} = 6.9 Hz), 1.52 (d, 3 H, PCH$_3$, J_{PH} = 4.5 Hz), 1.49 (d, 3 H, PCH$_3$, J_{PH} = 4.9 Hz), 1.47 (d, 3 H, PCH$_3$, J_{PH} = 5.3 Hz), 1.33 (d, 3 H, PCH$_3$, J_{PH} = 4.4 Hz), 0.93 (d, 3 H, PCH$_3$, J_{PH} = 3.3 Hz), 0.70 (d, 3 H, PCH$_3$, J_{PH} = 3.5 Hz) ppm (eight methylene protons are unaccounted for, vide supra); ^{31}P{^{1}H} NMR (121 MHz, C$_6$D$_6$) δ 24.5, 23.4, 10.4, −1.9 ppm; ^{13}C{^{1}H} NMR (75 MHz, C$_6$D$_6$) for 90% ^{13}CO-enriched material δ 252.4 (s), 250.8 (s) ppm. Anal. Calcd for C$_{34}$H$_{62}$ClO$_2$P$_4$TaZr: C, 43.70; H, 6.69; Cl, 3.79. Found: C, 43.22; H, 6.82; Cl, 3.91.

Reaction of [(dmpe)$_2$(CO)TaCOZrCp*$_2$Cl] (4) with 2 Equiv of Trimethylsilyl Chloride. To a solution of 0.119 g (0.127 mmol) of [(dmpe)$_2$(CO)TaCOZrCp*$_2$Cl] (**4**) in 6 mL of THF was added 32 μL (0.252 mmol) of Me$_3$SiCl. The reaction mixture was then stirred for 6 h, during which time the color of the solution changed from violet to green. The ^{31}P{^{1}H} NMR spectrum of the reaction mixture, reduced to dryness in vacuo and redissolved in C$_6$D$_6$, revealed only one peak at 25 ppm, indicative of [Ta(Me$_3$SiOCCOSiMe$_3$)(dmpe)$_2$Cl]; presumably, Cp*$_2$ZrCl$_2$ was also formed but no attempt was made to identify it.

Collection and Reduction of X-ray Data. [(dmpe)$_2$(CO)TaCOTa(*t*-BuMe$_2$SiOCCOSiMe$_2$-*t*-Bu)(dmpe)$_2$] (3b). Deep red crystals of this compound were grown by slow evaporation of a pentane solution at −30 °F. An irregularly shaped crystal was mounted under a nitrogen atmosphere in a Lindemann glass capillary using Apiezon grease. The crystal was judged to be acceptable on the basis of ω-scans of several low-angle reflections, which did not show any structure ($\Delta\bar{\omega}_{1/2}$ = 0.36°). Study on the diffractometer revealed $2/m$ Laue symmetry with systematic absences $h0l$, $l \neq 2n$, and $0k0$, $k \neq 2n$, consistent with space group $P2_1/c$ (C_{2h}^5, No. 14, cell choice 1).[9] Due to the lack of measurable faces, an empirical absorption correction was applied on the basis of azimuthal ψ-scans. Data collection proceeded in the usual manner for our laboratory,[10] details of which are given in Table I.

[(dmpe)$_2$(CO)TaCOZrCp*$_2$Cl] (4). A deep violet crystal of this complex was grown and mounted in a manner similar to that described above. The crystal was judged to be acceptable on the basis of ω-scans of several low-angle reflections which did not show any structure ($\Delta\bar{\omega}_{1/2}$ = 0.18°). Study on the diffractometer revealed only triclinic symmetry, consistent with either the space group $P1$ (C_1^1, No. 1) or $P\bar{1}$ (C_i^1, No. 2).[9] An empirical absorption correction was applied by using azimuthal ψ-scans. Data were collected as described elsewhere,[10] details of which are given in Table I.

Structure Determination and Refinement. All calculations were carried out using the TEXSAN program package.[11]

(8) Fieser, L. F.; Fieser, M. In *Reagents for Organic Synthesis*; John Wiley & Sons: New York, 1967; Vol. 1, pp 1033.

(9) (a) *International Tables for X-ray Crystallography*; Hahn, T., Ed.; D. Reidel: Dordrecht, 1983; pp 174–176. (b) *Ibid.*, p 82.

(10) Silverman, L. D.; Dewan, J. C.; Giandomenico, C. M.; Lippard, S. J. *Inorg. Chem.* **1980**, *19*, 3379.

(11) TEXSAN, a package of crystallographic programs supplied by the Molecular Structure Corp. All computations were made on a DEC VAXstation II 11/780 computer.

Table I. Experimental Details of the X-ray Diffraction Study of [(dmpe)$_2$(CO)TaCOTa(t-BuMe$_2$SiOCCOSiMe$_2$-t-Bu)(dmpe)$_2$] (3b) and [(dmpe)$_2$(CO)TaCOZrCp*$_2$Cl] (4)

	3b	4
formula	$C_{40}H_{94}O_4P_8Si_2Ta_2$	$C_{34}H_{62}ClO_2P_4TaZr$
a, Å	17.885 (8)	12.288 (2)
b, Å	21.041 (9)	17.851 (2)
c, Å	17.544 (5)	9.687 (2)
α, deg		90.67 (1)
β, deg	114.74 (3)	101.54 (1)
γ, deg		80.46 (1)
V, Å^3	5996 (8)	2053 (1)
fw	1305.04	934.38
Z	4	2
ρ_{calcd}, g/cm^3	1.352	1.51
space group	$P2_1/c$	$P\bar{1}$
radiation	Mo Kα	Mo Kα
data limits, deg	$3 < 2\theta < 44$, $+h,+k,\pm l$	$2 < 2\theta < 32$, $\pm h,\pm k,\pm l$ $32 < 2\theta < 50$, $+h,\pm k,\pm l$
crystal dim., mm	0.15 × 0.08 × 0.05	0.2 × 0.28 × 0.35
linear abs coeff, cm^{-1}	41.27	31.27
no. of data collected	7875	9508
no. of unique data [$F > 6\sigma(F)$]	3648	5828
no. of params	385	388
R_1[a]	0.051	0.026
R_2[a]	0.072	0.036

[a] $R_1 = \sum||F_o| - |F_c||/\sum|F_o|$; $R_2 = [\sum w||F_o| - |F_c||^2/\sum_w|F_o|^2]^{1/2}$, where $w = 1/\sigma^2(F_o)$. For more details see ref 10.

[(dmpe)$_2$(CO)TaCOTa(t-BuMe$_2$SiOCCOSiMe$_2$-t-Bu)(dmpe)$_2$] (3b). The positions of the tantalum atoms were determined by direct methods, and all remaining non-hydrogen atoms were located from a series of difference Fourier maps. All of the non-hydrogen atoms except the carbon atoms of the dmpe ligands were assigned anisotropic thermal parameters. All hydrogen atoms were placed in calculated positions (d_{C-H} = 0.95 Å) and allowed to "ride" on the appropriate carbons, with B(H) = 1.2B_{eq}(C). The function minimized during refinement was $\sum w(|F_o| - |F_c|)^2$ where $w = 1/\sigma^2(F_o)$. Refinement in this manner yielded the R factors given in Table I. The largest ratio of parameter shift to estimated standard deviation in the final cycle of refinement was less than 0.15, and the largest peak in the difference Fourier map was 1.50 e/Å^3, located near P(7). Final non-hydrogen atom positional and equivalent thermal parameters are given in Table II. Final non-hydrogen atom thermal parameters, hydrogen atom positional and thermal parameters, and a listing of observed and calculated structure factors are given in Tables S1–S3 (supplementary material), respectively.

[(dmpe)$_2$(CO)TaCOZrCp*$_2$Cl] (4). The position of the tantalum atom was determined from a Patterson synthesis and all of the remaining non-hydrogen atoms were located from a series of difference Fourier maps. All non-hydrogen atoms were refined with anisotropic thermal parameters. All hydrogen atoms were placed in calculated positions (d_{C-H} = 0.95 Å) and allowed to "ride" on the appropriate carbon atoms, with B(H) = 1.2B_{eq}(C). The function minimized during refinement was $\sum w(|F_o| - |F_c|)^2$ where $w = 1/\sigma^2(F_o)$. Refinement in this manner yielded the R factors given in Table I. The largest ratio of parameter shift to estimated standard deviation in the final cycle of refinement was 0.05, and the largest peak in the difference Fourier map was 0.50 e/Å^3, located near C(21). Final non-hydrogen atom positional and equivalent isotropic thermal parameters are given in Table III. Final non-hydrogen atom thermal parameters, hydrogen atom positional and thermal parameters, and a listing of observed and calculated structure factors are given in Tables S4–S6 (supplementary material), respectively.

Results

Reaction of Na[Ta(CO)$_2$(dmpe)$_2$] with Me$_3$SiCl. When 1 equiv of trimethylsilyl chloride is allowed to react with the sodium salt of the [Ta(CO)$_2$(dmpe)$_2$]$^-$ anion (**5**), the siloxycarbyne complex, [Ta(≡COSiMe$_3$)(CO)(dmpe)$_2$] (**2a**), forms immediately.[4,5] If the reaction mixture is allowed to stir for a slightly longer period of time, this compound is converted into the CO-bridged complex

Table II. Final Non-Hydrogen Atom Positional and Equivalent Thermal Parameters for [(dmpe)$_2$(CO)TaCOTa(t-BuMe$_2$SiOCCOSiMe$_2$-t-Bu)(dmpe)$_2$] (3b)[a]

atom	x	y	z	B(eq),[b] Å^2
Ta(1)	0.60321 (5)	0.11794 (4)	0.79497 (5)	3.14 (4)
Ta(2)	0.27975 (5)	0.09503 (4)	0.71753 (5)	3.49 (4)
P(1)	0.6425 (4)	0.1120 (3)	0.9529 (3)	4.9 (3)
P(2)	0.5723 (3)	0.0041 (3)	0.8209 (3)	3.8 (2)
P(3)	0.5717 (4)	0.2350 (3)	0.7736 (5)	5.5 (3)
P(4)	0.5447 (4)	0.1277 (3)	0.6360 (3)	5.3 (3)
P(5)	0.3002 (4)	0.1573 (3)	0.8449 (4)	5.7 (3)
P(6)	0.1460 (5)	0.0726 (5)	0.7335 (7)	9.7 (5)
P(7)	0.2222 (5)	0.1828 (4)	0.6101 (6)	8.6 (4)
P(8)	0.2281 (4)	0.0371 (4)	0.5805 (4)	6.4 (3)
Si(1)	0.8607 (4)	0.2193 (3)	0.8588 (4)	5.7 (3)
Si(2)	0.8008 (4)	0.0002 (3)	0.7606 (4)	4.6 (3)
O(1)	0.7698 (8)	0.1932 (6)	0.7968 (8)	4.9 (6)
O(2)	0.7816 (8)	0.0400 (6)	0.8303 (7)	4.1 (6)
O(3)	0.4721 (9)	0.1186 (6)	0.7678 (9)	4.3 (6)
O(4)	0.332 (1)	−0.0409 (8)	0.808 (1)	6.9 (9)
C(1)	0.716 (1)	0.146 (1)	0.803 (1)	4 (1)
C(2)	0.721 (1)	0.085 (1)	0.814 (1)	4 (1)
C(3)	0.395 (1)	0.1086 (8)	0.739 (1)	4 (1)
C(4)	0.313 (1)	0.008 (1)	0.778 (1)	5 (1)
C(11)	0.595 (1)	0.044 (1)	0.979 (1)	6.0 (5)
C(12)	0.756 (2)	0.101 (1)	1.016 (2)	7.6 (7)
C(13)	0.629 (2)	0.171 (1)	1.020 (2)	7.9 (7)
C(21)	0.537 (1)	0.009 (1)	0.906 (1)	4.7 (5)
C(22)	0.490 (1)	−0.043 (1)	0.742 (1)	4.8 (5)
C(23)	0.653 (2)	−0.054 (1)	0.863 (2)	6.9 (6)
C(31)	0.534 (2)	0.252 (2)	0.658 (3)	12 (1)
C(32)	0.648 (2)	0.297 (2)	0.825 (2)	9.4 (8)
C(33)	0.490 (2)	0.265 (1)	0.796 (2)	6.8 (6)
C(41)	0.491 (2)	0.206 (2)	0.608 (2)	8.6 (8)
C(42)	0.463 (2)	0.077 (2)	0.564 (2)	11 (1)
C(43)	0.618 (2)	0.133 (1)	0.591 (2)	8.6 (8)
C(51)	0.228 (2)	0.139 (2)	0.892 (2)	10 (1)
C(52)	0.393 (2)	0.147 (1)	0.938 (2)	8.4 (7)
C(53)	0.302 (2)	0.245 (2)	0.844 (2)	10 (1)
C(61)	0.157 (3)	0.125 (2)	0.834 (3)	16 (1)
C(62)	0.040 (2)	0.091 (2)	0.665 (2)	9.7 (9)
C(63)	0.128 (2)	−0.005 (2)	0.761 (2)	11 (1)
C(71)	0.210 (3)	0.144 (3)	0.498 (3)	18 (2)
C(72)	0.280 (2)	0.255 (1)	0.606 (2)	8.6 (8)
C(73)	0.125 (2)	0.223 (2)	0.586 (2)	9.6 (8)
C(81)	0.199 (3)	0.082 (3)	0.491 (3)	18 (2)
C(82)	0.287 (2)	−0.023 (1)	0.558 (2)	7.8 (7)
C(83)	0.128 (3)	−0.009 (3)	0.555 (3)	17 (2)
C(101)	0.858 (2)	0.265 (2)	0.948 (2)	9 (2)
C(102)	0.932 (2)	0.152 (1)	0.904 (2)	9 (2)
C(103)	0.894 (1)	0.270 (1)	0.791 (2)	8 (2)
C(104)	0.972 (2)	0.306 (2)	0.849 (2)	13 (2)
C(105)	0.825 (2)	0.320 (2)	0.745 (2)	13 (2)
C(106)	0.904 (3)	0.227 (2)	0.721 (3)	17 (3)
C(201)	0.837 (2)	0.056 (1)	0.698 (1)	7 (1)
C(202)	0.712 (2)	−0.042 (1)	0.688 (2)	9 (2)
C(203)	0.887 (1)	−0.057 (1)	0.827 (2)	6 (1)
C(204)	0.966 (2)	−0.020 (1)	0.877 (2)	8 (2)
C(205)	0.858 (2)	−0.095 (2)	0.882 (2)	10 (2)
C(206)	0.906 (2)	−0.099 (2)	0.763 (2)	11 (2)

[a] Numbers in parentheses are errors in the last significant digit(s). See Figure 1 for atom-labeling scheme. [b] B(eq) = $^4/_3[a^2\beta_{11} + b^2\beta_{22} + c^2\beta_{33} + (2ab\cos\gamma)\beta_{12} + (2ac\cos\beta)\beta_{13} + (2bc\cos\alpha)\beta_{23}]$.

[(dmpe)$_2$(CO)TaCOTa(Me$_3$SiOCCOSiMe$_3$)(dmpe)$_2$] (**3a**), eq 3. The presence of sodium chloride appears to be essential for this reaction. If the tetra-n-hexylammonium salt of the anion is allowed to react with 1 equiv of Me$_3$SiCl, the only product observed is the siloxycarbyne,

$$\mathrm{Na[Ta(CO)_2(dmpe)_2]} \xrightarrow{\mathrm{Me_3SiCl}} \underset{\mathbf{5}}{} \mathrm{[Ta(\equiv C{-}OSiMe_3)(CO)(dmpe)_2]} + \mathrm{NaCl} \rightarrow \underset{\mathbf{2a}}{} \mathrm{[(dmpe)_2(CO)Ta{=}C{=}O{-}Ta(Me_3SiOC{\equiv}COSiMe_3)(dmpe)_2]} \quad (3)$$

Table III. Final Non-Hydrogen Atom Positional and Equivalent Thermal Parameters for [(dmpe)$_2$(CO)TaCOZrCp*$_2$Cl] (4)[a]

atom	x	y	z	B(eq),[b] Å^2
Ta	0.06410 (2)	0.15645 (1)	0.19353 (1)	2.36 (1)
Zr	0.40201 (4)	−0.20655 (3)	0.32699 (2)	2.30 (2)
Cl	0.3222 (2)	−0.1773 (2)	0.45511 (8)	5.2 (1)
P(1)	−0.0656 (2)	0.1709 (1)	0.31561 (8)	3.89 (8)
P(2)	0.1593 (2)	0.3117 (1)	0.2445 (1)	4.36 (9)
P(3)	0.1891 (1)	0.1698 (1)	0.06921 (7)	3.51 (7)
P(4)	−0.1230 (1)	0.2955 (1)	0.10061 (8)	3.66 (7)
O(1)	0.2806 (3)	−0.0622 (3)	0.2745 (2)	3.3 (2)
O(2)	−0.0989 (5)	−0.0223 (4)	0.1428 (3)	6.1 (3)
C(1)	0.2007 (5)	0.0286 (4)	0.2434 (3)	2.7 (2)
C(2)	−0.0403 (5)	0.0442 (4)	0.1622 (3)	3.4 (3)
C(11)	0.018 (1)	0.246 (1)	0.3764 (3)	9.9 (9)
C(12)	−0.2478 (8)	0.2459 (6)	0.3164 (4)	6.4 (5)
C(13)	−0.0766 (8)	0.0451 (7)	0.3829 (4)	6.6 (5)
C(21)	0.073 (2)	0.334 (1)	0.3366 (6)	12 (1)
C(22)	0.134 (1)	0.4579 (6)	0.1997 (6)	8.9 (6)
C(23)	0.342 (1)	0.2900 (7)	0.2709 (7)	9.4 (7)
C(31)	0.0689 (7)	0.2421 (6)	−0.0119 (3)	5.7 (4)
C(32)	0.3363 (8)	0.2442 (7)	0.0508 (4)	6.6 (5)
C(33)	0.2641 (8)	0.0397 (6)	0.0342 (3)	5.6 (4)
C(41)	−0.0368 (8)	0.3321 (6)	0.0097 (4)	6.2 (4)
C(42)	−0.212 (1)	0.4377 (7)	0.1117 (5)	7.9 (6)
C(43)	−0.2698 (9)	0.2422 (7)	0.0713 (6)	8.5 (6)
C(51)	0.3925 (5)	−0.3740 (4)	0.2624 (3)	3.3 (3)
C(52)	0.3792 (5)	−0.4143 (4)	0.3416 (3)	3.3 (3)
C(53)	0.2494 (6)	−0.3580 (4)	0.3640 (3)	3.4 (3)
C(54)	0.1826 (5)	−0.2808 (4)	0.3022 (3)	3.3 (3)
C(55)	0.2709 (5)	−0.2908 (4)	0.2389 (3)	3.2 (3)
C(61)	0.4936 (7)	−0.4299 (5)	0.2103 (4)	5.0 (4)
C(62)	0.4754 (7)	−0.5111 (5)	0.3890 (4)	4.6 (3)
C(63)	0.1854 (7)	−0.3868 (6)	0.4405 (4)	5.4 (4)
C(64)	0.0393 (6)	−0.2079 (5)	0.3005 (4)	5.6 (4)
C(65)	0.2337 (8)	−0.2293 (6)	0.1591 (3)	5.4 (4)
C(71)	0.6381 (5)	−0.2023 (4)	0.2615 (3)	3.1 (3)
C(72)	0.5845 (5)	−0.0921 (4)	0.2743 (3)	3.0 (2)
C(73)	0.5827 (5)	−0.0936 (4)	0.3538 (3)	3.3 (3)
C(74)	0.6381 (5)	−0.2053 (5)	0.3896 (3)	3.6 (3)
C(75)	0.6726 (5)	−0.2723 (4)	0.3330 (3)	3.5 (3)
C(81)	0.6836 (7)	−0.2296 (5)	0.1850 (4)	5.0 (4)
C(82)	0.5491 (7)	0.0097 (5)	0.2140 (3)	4.6 (3)
C(83)	0.5361 (8)	0.0063 (6)	0.3931 (4)	5.5 (4)
C(84)	0.6741 (8)	−0.2399 (7)	0.4732 (4)	6.5 (5)
C(85)	0.7620 (7)	−0.3904 (5)	0.3452 (5)	5.9 (4)

[a] Numbers in parentheses are errors in the last significant digit(s). See Figure 5 for atom-labeling scheme. [b] $B(\text{eq}) = {}^4/_3[a^2\beta_{11} + b^2\beta_{22} + c^2\beta_{33} + (2ab\cos\gamma)\beta_{12} + (2ac\cos\beta)\beta_{13} + (2bc\cos\alpha)\beta_{23}]$.

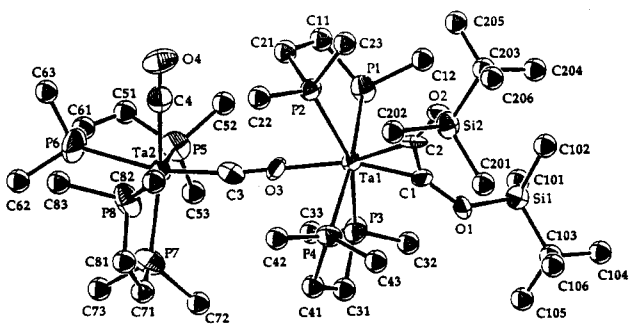

Figure 1. Structure of [(dmpe)$_2$(CO)TaCOTa(*t*-BuMe$_2$SiOCCOSiMe$_2$-*t*-Bu)(dmpe)$_2$] (**3b**), showing the 40% thermal ellipsoids and atom-labeling scheme. The carbon atoms of the dmpe groups have been depicted as spheres with $B = 5$ Å^2 for clarity.

even after prolonged reaction times.

Addition of 2 equiv of Me_3SiCl to a solution containing **3a** affords 2 equiv of the mononuclear complex [Ta(Me$_3$SiOCCOSiMe$_3$)(dmpe)$_2$Cl]. In a similar reaction, **3a** was allowed to react with NaI in THF over a period of 2 days, which resulted in the formation of a mixture of

Table IV. Interatomic Distances (Å) and Angles (deg) for [(dmpe)$_2$(CO)TaCOTa(*t*-BuMe$_2$SiOCCOSiMe$_2$-*t*-Bu)(dmpe)$_2$] (3b)[a]

Bond Distances			
Ta(1)–C(2)	2.11 (2)	Ta(2)–P(5)	2.481 (6)
Ta(1)–C(1)	2.05 (2)	Ta(2)–P(6)	2.565 (7)
Ta(1)–O(3)	2.19 (1)	Ta(2)–P(8)	2.502 (6)
Ta(1)–P(4)	2.545 (5)	Si(1)–O(1)	1.63 (1)
Ta(1)–P(2)	2.541 (5)	Si(2)–O(2)	1.63 (1)
Ta(1)–P(3)	2.520 (6)	O(1)–C(1)	1.41 (2)
Ta(1)–P(1)	2.561 (5)	O(2)–C(2)	1.38 (2)
Ta(2)–C(3)	1.96 (2)	O(3)–C(3)	1.27 (2)
Ta(2)–C(4)	2.08 (2)	O(4)–C(4)	1.14 (3)
Ta(2)–P(7)	2.530 (7)	C(1)–C(2)	1.30 (3)

Bond Angles			
C(2)–Ta(1)–C(1)	36.4 (8)	C(4)–Ta(2)–P(7)	165.0 (6)
C(2)–Ta(1)–O(3)	160.0 (6)	C(4)–Ta(2)–P(5)	95.7 (6)
C(2)–Ta(1)–P(4)	97.1 (5)	C(4)–Ta(2)–P(6)	81.8 (6)
C(2)–Ta(1)–P(2)	86.5 (6)	C(4)–Ta(2)–P(8)	88.5 (6)
C(2)-Ta(1)-P(3)	119.5 (6)	P(7)–Ta(2)–P(5)	98.4 (3)
C(2)–Ta(1)–P(1)	90.7 (5)	P(7)–Ta(2)–P(6)	96.2 (3)
C(1)–Ta(1)–O(3)	161.2 (7)	P(7)–Ta(2)–P(8)	76.6 (3)
C(1)–Ta(1)–P(4)	89.7 (5)	P(5)–Ta(2)–P(6)	78.0 (3)
C(1)–Ta(1)–P(2)	122.9 (6)	P(5)–Ta(2)–P(8)	168.1 (2)
C(1)–Ta(1)–P(3)	83.0 (7)	P(6)–Ta(2)–P(8)	91.7 (3)
C(1)–Ta(1)–P(1)	97.0 (5)	C(3)–Ta(2)–C(4)	88.9 (8)
O(3)–Ta(1)–P(4)	81.3 (4)	C(3)–Ta(2)–P(7)	96.1 (6)
O(3)–Ta(1)–P(2)	75.6 (4)	C(3)–Ta(2)–P(5)	90.1 (5)
O(3)–Ta(1)–P(3)	79.0 (4)	C(3)–Ta(2)–P(6)	164.0 (6)
O(3)–Ta(1)–P(1)	91.1 (4)	C(3)–Ta(2)–P(8)	101.1 (6)
P(4)–Ta(1)–P(2)	104.6 (2)	C(1)–O(1)–Si(1)	135 (1)
P(4)–Ta(1)–P(3)	78.1 (2)	C(2)–O(2)–Si(2)	126 (1)
P(4)–Ta(1)–P(1)	172.2 (2)	C(3)–O(3)–Ta(1)	166 (1)
P(2)–Ta(1)–P(3)	153.6 (2)	C(2)–C(1)–O(1)	134 (2)
P(2)–Ta(1)–P(1)	75.0 (2)	C(2)–C(1)–Ta(1)	70 (1)
P(3)–Ta(1)–P(1)	98.7 (2)	O(1)–C(1)–Ta(1)	151 (2)
C(1)–C(2)–O(2)	135 (2)	O(3)–C(3)–Ta(2)	169 (2)
C(1)–C(2)–Ta(1)	70 (1)	O(4)–C(4)–Ta(2)	176 (2)
O(2)–C(2)–Ta(1)	155 (1)		

Intraligand Geometry

bond or angle type	min	max	mean
P-C	1.72 (6)	2.05 (6)	1.84 (3)
Si-C	1.80 (3)	1.92 (3)	1.86 (3)
(P)C-C(P)	1.28 (5)	1.47 (3)	1.35 (5)
C-C	1.50 (4)	1.60 (5)	1.55 (4)
Ta-P-C	104 (1)	131 (1)	117 (1)
C-P-C	96 (1)	105 (2)	101 (2)
P-C-C	110 (3)	121 (4)	115 (3)
O-Si-C	103.4 (9)	112 (1)	109 (1)
C-Si-C	107 (1)	112 (2)	110 (1)
Si-C-C	106 (2)	110 (2)	109 (2)
C-C-C	105 (2)	113 (3)	110 (3)

[a] Numbers in parentheses are estimated standard deviations in the last digit(s) given. Standard deviations quoted for the mean value are the average deviations for the individual values.

Na[Ta(CO)$_2$(dmpe)$_2$] (**5**) and [Ta(Me$_3$SiOCCOSiMe$_3$)(dmpe)$_2$I], as evidenced by the phosphorus NMR signals at 22.6, 8.0, and 15.0 ppm, respectively; decomposition products were also observed.

Structural studies were performed on the *tert*-butyldimethylsilyl analogue, [(dmpe)$_2$(CO)TaCOTa(*t*-BuMe$_2$SiOCCOSiMe$_2$-*t*-Bu)(dmpe)$_2$] (**3b**), since it was not possible to obtain X-ray-quality crystals of **3a**. This compound was prepared in a manner identical to that used to prepare **3a**. An ORTEP diagram of **3b** is shown in Figure 1; selected bond distances and angles are summarized in Table IV. The geometric environment about Ta(1) is best described as distorted octahedral, with the midpoint of the acetylene bond trans to O(3) occupying one vertex. Distortion from idealized geometry is caused by the small bite angles of the dmpe ligands and a tilting of the phosphines toward O(3) owing to steric interactions with the bulky *tert*-butyldimethylsilyl groups on the acetylene. The ge-

ometry about Ta(2) is also distorted octahedral, with the terminal and bridging carbonyls cis to one another. Again distortions arise from the chelating nature of the dmpe ligands. The carbonyl bridge in **3b** is remarkably linear with bond angles of 169 (2) and 166 (1)° for Ta(2)=C(3)=O(3) and Ta(1)—O(3)=C(3), respectively. As observed in the complexes $[M(Me_3SiOCCOSiMe_3)(dmpe)_2X]$ (M = Nb, X = Cl; M = Ta, X = Cl or OTf),[12,13] the acetylene ligand is aligned parallel to one of the trans P—Ta—P vectors. This eclipsed conformation may be the result of intramolecular packing forces that minimize steric interactions between the dmpe methyl and the silyl alkyl groups. Electronic factors, in which favorable interactions of metal d orbitals with the acetylene π^* orbital occur in this conformation, may also be involved. Such an effect is seen in the structure of $[Ta(CO)_2(PMe_3)_2(PhCCPh)I]$,[14] in which the acetylene is aligned along the trans OC—Ta—CO vector.

The acetylene C—C distance of 1.30 (3) Å found in **3b** is shorter by 0.06 and 0.04 Å, respectively, than those found in the bis(trimethylsiloxy)acetylene complexes $[Ta(Me_3SiOCCOSiMe_3)(dmpe)_2X]$ (X = Cl or OTf).[12,13] Interestingly, the acetylene C—C distance in **3b** is close to the value of 1.28 (1) Å found in the dihydroxyacetylene complex, $[TaH(HOCCOH)(dmpe)_2Cl]Cl$.[15] It is difficult to draw firm conclusions from these comparisons, however, in view of the relatively large estimated standard deviation in the C≡C distance. The average acetylene Ta—C distance of 2.05 (2) Å in **3b** is in excellent agreement with the corresponding values of 2.065 (5), 2.07 (1), and 2.08 (7) Å found in $[Ta(Me_3SiOCCOSiMe_3)(dmpe)_2Cl]$,[13] $[Ta(Me_3SiOCCOSiMe_3)(dmpe)_2OTf]$,[13] and $[TaH(HOCCOH)(dmpe)_2Cl]Cl$,[15] respectively. The difference between Ta(1)—C(1) (2.05 (2) Å) and Ta(1)—C(2) (2.11 (2) Å), although not statistically significant, may be due to steric interactions between the dmpe methyls and the bulky *tert*-butyl groups on the silicon atom. The 9° difference between C(2)—O(2)—Si(2), 126 (1)°, and C(1)—O(1)—Si(1), 135 (1)°, may also be due to these same steric interactions.

Bond distances found in the bridging carbonyl group indicate significant diminution of the normal C≡O triple-bond character. The 1.96 (2) Å distance for Ta(2)—C(3) is 0.12 Å shorter than Ta(2)—C(4) (2.08 (2) Å) for the terminal carbonyl group, but 0.11 Å longer than the formal Ta—C triple bond distance of 1.85 (1) Å found in $[Ta\{\equiv COSi(i\text{-}Pr)_3\}(CO)(dmpe)_2]$ (**2b**).[4] Also, the bridging C(3)—O(3) distance of 1.27 (2) Å is 0.13 Å longer than that found in the terminal carbonyl, 1.14 (2) Å, and 0.07 Å shorter than the C—O single bond, 1.34 (2) Å, in **2**.[4] The electronic delocalization implied by these geometric parameters (eq 4) is also manifested in the FTIR spectrum,

$$\underset{\mathbf{A}}{Ta(2)\equiv C-O-Ta(1)} \leftrightarrow \underset{\mathbf{B}}{Ta(2)=C=O-Ta(1)} \leftrightarrow \underset{\mathbf{C}}{Ta(2)-C\equiv O-Ta(1)} \quad (4)$$

where the frequency for the bridging carbonyl appears at the unusually low value of 1462 cm^{-1}, as determined by ^{13}CO labeling.

The $^{31}P\{^1H\}$ NMR spectrum of **3a** shown in Figure 2 consists of two sets of resonances with splitting patterns

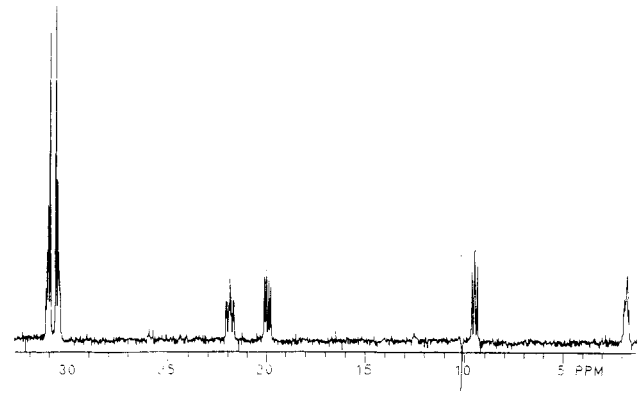

Figure 2. $^{31}P\{^1H\}$ NMR spectrum of $[(dmpe)_2(CO)TaCOTa(Me_3SiOCCOSiMe_3)(dmpe)_2]$ (**3a**) dissolved in C_6D_6.

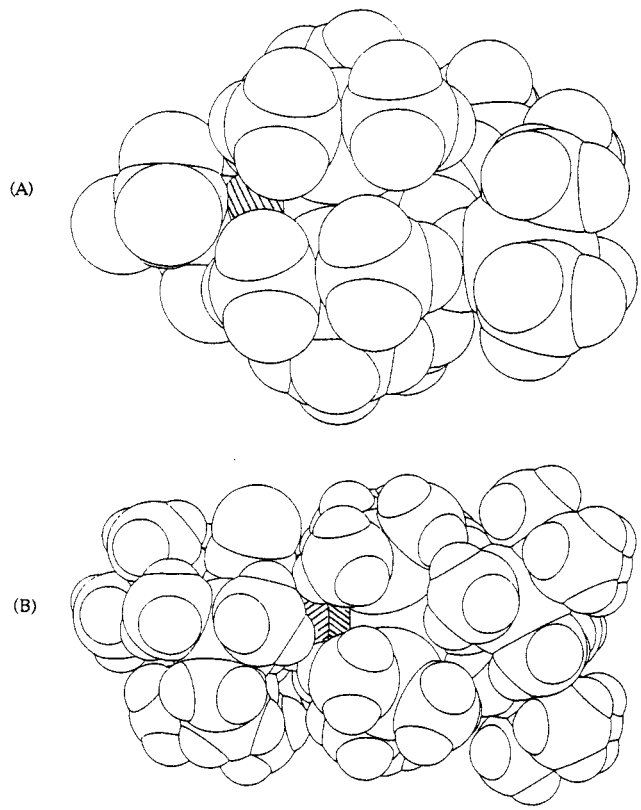

Figure 3. Space-filling models of (A) $[Ta(Me_3SiOCCOSiMe_3)(dmpe)_2OTf]$, in which the oxygen atom linking the Ta and S centers is shaded, and (B) $[(dmpe)_2(CO)TaCOTa(t\text{-}BuMe_2SiOCCOSiMe_2\text{-}t\text{-}Bu)(dmpe)_2]$ (**3b**), in which the bridging CO ligand is shaded.

characteristic of dmpe phosphorus atoms bound to the two different tantalum centers. The AA′BB′ splitting pattern in the most downfield region is assigned to phosphines coordinated to Ta(1). These phosphorus nuclei are chemically inequivalent owing to hindered rotation about the Ta(1)–O(3) bond, a result of steric interactions with the dmpe groups bound to Ta(2). In contrast, in $[Ta(Me_3SiOCCOSiMe_3)(dmpe)_2OTf]$,[12,13] where the ^{31}P NMR chemical shifts of the phosphines are approximately the same as in **3a**, no such AA′BB′ splitting pattern is seen at room temperature. This difference is presumably due to free rotation about the Ta–OTf bond in the latter compound, which has less steric restriction. This effect is illustrated for the *tert*-butyldimethylsilyl analogue **3b** in Figure 3, which displays space-filling diagrams. From the figure, it is apparent that the dmpe methyl groups on the two different sides of the carbonyl bridge in **3b**, and by

(12) Bianconi, P. A.; Williams, I. D.; Engeler, M. P.; Lippard, S. J. *J. Am. Chem. Soc.* **1986**, *108*, 311.
(13) Bianconi, P. A.; Vrtis, R. N.; Rao, C. P.; Williams, I. D.; Engeler, M. P.; Lippard, S. J. *Organometallics* **1987**, *6*, 1968.
(14) McGeary, M. J.; Gamble, A. S.; Templeton, J. L. *Organometallics* **1988**, *7*, 271.
(15) Vrtis, R. N.; Rao, C. P.; Bott, S. G.; Lippard, S. J. *J. Am. Chem. Soc.* **1988**, *110*, 7564.

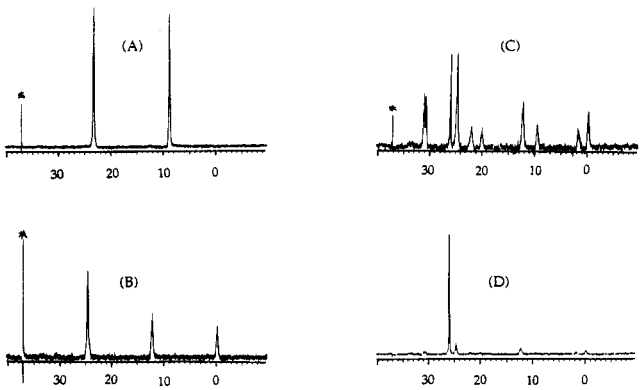

Figure 4. Time dependence of the $^{31}P\{^1H\}$ NMR spectrum of $Na[Ta(CO)_2(dmpe)_2]$ in THF-d_8, following addition of 1 equiv of Me_3SiCl at t = 0 min and a second equivalent at t = 150 min. The asterisk denotes a glitch in the spectrometer output: (A) 0 min; (B) 1 min; (C) 120 min; (D) 360 min.

implication **3a**, are interlocked, freezing the compound into one rotational conformation.

The $^{31}P\{^1H\}$ NMR spectrum of **3a** also exhibits four resonances at 21.7, 19.8, 9.1, and 1.5 ppm split into a ABMX pattern (Figure 2), similar to that seen for $[Ta\{\equiv COSi(i\text{-}Pr)_3\}(CO)(dmpe)_2]$, in which the resonances occur at 25.4, 24.7, 11.7, and −0.6 ppm.[4] The differences in chemical shifts reflect slight differences in electron density at the metal center.

Figure 4 shows the results of a time-dependent $^{31}P\{^1H\}$ NMR experiment in which 1 equiv of Me_3SiCl was added via syringe to an NMR tube containing a solution of $Na[Ta(CO)_2(dmpe)_2]$ in THF-d_8. Upon addition of the Me_3SiCl, $[Ta(\equiv COSiMe_3)(CO)(dmpe)_2]$ formed immediately, as judged by its characteristic $^{31}P\{^1H\}$ NMR pattern (Figure 4B).[5] Over a period of 2 h, the spectrum of this mixture slowly changed, with peaks attributable to **3a** and $[Ta(Me_3SiOCCOSiMe_3)(dmpe)_2Cl]$ appearing as the peaks resulting from the siloxycarbyne decreased in intensity (Figure 4C). After 2.5 h, a second equivalent of Me_3SiCl was added to the NMR tube. At the end of 6 h, the major resonance observed was that of $[Ta(Me_3SiOCCOSiMe_3)(dmpe)_2Cl]$, with some residual CO-bridged complex, **3a**, still present (Figure 4D).

The $^{13}C\{^1H\}$ NMR spectrum of 90% ^{13}CO-enriched **3a** consists of three resonances. The chemical shift of the most upfield resonance, 210.2 ppm, a quintet (J_{PC} = 17 Hz) due to coupling to the four phosphorus atoms, is similar to the chemical shift of 212.5 ppm observed for the disiloxyacetylene ligand in $[Ta(Me_3SiOCCOSiMe_3)(dmpe)_2Cl]$.[12,13] The two further downfield resonances at 257.2 and 247.6 ppm are assigned to the terminal and bridging carbonyls, respectively, and are similar in chemical shift to the resonances at 253.2 and 243.4 ppm observed for $[Ta\{\equiv COSi(i\text{-}Pr)_3\}(CO)(dmpe)_2]$.[5] This result further confirms the significant electronic delocalization characteristic of a bridging carbonyl in **3a,b**, which has metal oxycarbyne character.

Reaction of $Na[Ta(CO)_2(dmpe)_2]$ with $Cp^*_2ZrCl_2$. When 1 equiv of $Cp^*_2ZrCl_2$ was added to a solution of $Na[Ta(CO)_2(dmpe)_2]$ (**5**) in THF, the violet complex $[(dmpe)_2(CO)TaCOZrCp^*_2Cl]$ (**4**) formed rapidly. As was the case for **3a**, complex **4** reacts with 2 equiv of Me_3SiCl, yielding the coupled product $[Ta(Me_3SiOCCOSiMe_3)(dmpe)_2Cl]$. Presumably, $Cp^*_2ZrCl_2$ also forms in this reaction, although this product was not isolated.

An ORTEP diagram of **4** is shown in Figure 5. As observed for **3b** there is a nearly linear carbonyl bridge between the metal centers, with the carbon atom bound to

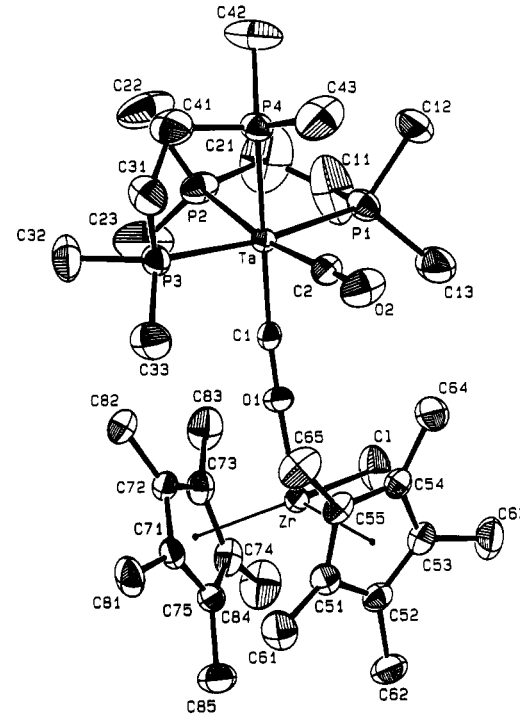

Figure 5. Structure of $[(dmpe)_2(CO)TaCOZrCp^*_2Cl]$ (**4**), showing the 40% thermal ellipsoids and atom-labeling scheme.

tantalum and the oxygen atom coordinated to zirconium. The geometry about the tantalum atom is best described as distorted octahedral, the distortion arising from the two chelating dmpe ligands which have acute bite angles. The zirconium atom is in a tetrahedral environment where two vertices are occupied by the centroids of the Cp* ligands.

Selected bond distances and angles for **4** are displayed in Table V. The carbonyl bridge in **4** is more linear than that in **3b**, with bond angles of 173.5 (4) and 177.8 (3)° for Ta—C(1)—O(1) and Zr—O(1)—C(1), respectively. The bridging Ta—C bond (1.935 (5) Å) is shorter than that to the terminal carbonyl (2.016 (5) Å), a difference identical to that observed for **3b**. Unlike **3b**, however, the bridging C(1)—O(1) bond (1.269 (6) Å) in **4** is lengthened with respect to the terminal carbonyl (1.181 (6) Å) by only 0.088 Å, whereas in **3b** the difference is 0.14 Å.

The $^{31}P\{^1H\}$ NMR spectrum of **4** consists of four resonances at 24.5, 23.5, 10.4, and −1.9 ppm, forming an ABMX pattern. This $^{31}P\{^1H\}$ NMR spectrum is almost identical to that of $[Ta\{\equiv COSi(i\text{-}Pr)_3\}(CO)(dmpe)_2]$ (**2**),[4,5] which has resonances at 25.4, 24.7, 11.7, and −0.6 ppm. The $^{13}C\{^1H\}$ NMR spectrum of 90% ^{13}CO-enriched **4** exhibits two resonances at 252.4 and 250.8 ppm for the terminal and bridging carbonyl carbon atoms, respectively. The asymmetry of **4** is evidenced by the inequivalence of the protons on the two Cp* ligands, which appear at 2.06 and 2.05 ppm in the ^1H NMR spectrum.

Discussion

Formation of $[(dmpe)_2(CO)TaCOTa(Me_3SiOCCOSiMe_3)(dmpe)_2]$ (3a). The carbonyl-bridged complex **3a** appears to form directly from two siloxycarbyne complexes $[Ta(\equiv COSiMe_3)(CO)(dmpe)_2]$ (**2a**). This process is promoted by the presence of NaCl in solution and will not occur when the salt is $(n\text{-}C_6H_{13})_4NCl$. The mechanism involved in this reaction is currently unknown, but one possibility is given in eq 5. The first step in this reaction pathway is desilation of the siloxycarbyne (**2**) in the presence of NaCl, yielding $Na[Ta(CO)_2(dmpe)_2]$ (**5**) and Me_3SiCl, the reversal of the

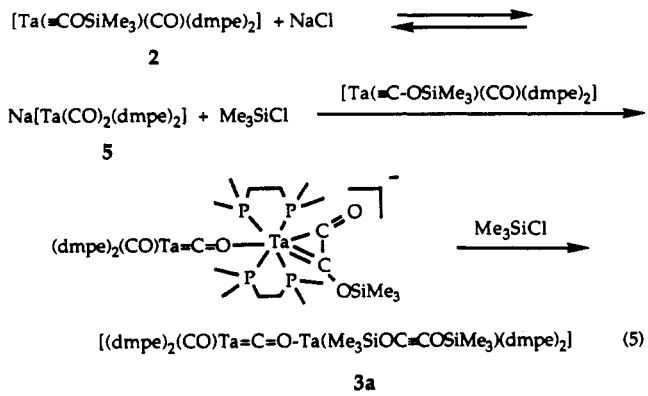

(5)

reaction involved in forming the siloxycarbyne.[4] This step is favored by the presence of sodium, rather than tetra-*n*-hexylammonium, chloride because the anion would be better stabilized through interaction of its electron-rich carbonyl oxygen atoms with the stronger Lewis acid, Na^+. The next step in the postulated mechanism is electrophilic attack at the carbonyl oxygen atom of the anion by the siloxycarbyne, forming a putative CO-bridged η^2-ketenyl dimetallic transition state or intermediate. Analogous η^2-ketenyl species may form along the mechanistic pathway in the reaction of $[Ta(\equiv COSiR_3)(CO)(dmpe)_2]$ with R_3SiCl to yield $[Ta(R_3SiOCCOSiR_3)(dmpe)_2Cl]$,[16] although other mechanisms are possible.[1,17] Preferential reaction of $Na[Ta(CO)_2(dmpe)_2]$ (**5**) with the siloxycarbyne rather than Me_3SiCl may be due to relative stabilities of the final products in the absence of excess silyl chloride. In the final step of the proposed pathway a second equivalent of Me_3SiCl converts the bridged carbonyl η^2-ketenyl intermediate into the observed product **3**, with regeneration of NaCl.

The carbonyl-bridged complex **3a** will react with additional Me_3SiCl to produce $[Ta(Me_3SiOCCOSiMe_3)(dmpe)_2Cl]$, the product observed in the reaction of $Na[Ta(CO)_2(dmpe)_2]$ (**5**) with 2 equiv of Me_3SiCl.[12,13] Compound **3a** does not appear to be a required intermediate in the formation of $[Ta(Me_3SiOCCOSiMe_3)(dmpe)_2Cl]$, however, since the related siloxycarbyne $[Ta\{\equiv COSi(i\text{-}Pr)_3\}(CO)(dmpe)_2]$ reacts with 1 equiv of Me_3SiCl in THF, yielding $[Ta\{Me_3SiOCCOSi(i\text{-}Pr)_3\}(dmpe)_2Cl]$ as the only product.[18] For the asymmetric product to be formed exclusively via a bridged complex would require the reaction of $[Ta\{\equiv COSi(i\text{-}Pr)_3\}(CO)(dmpe)_2]$ with $[Ta(\equiv COSiMe_3)(CO)(dmpe)_2]$ to be much more favorable than reaction with either siloxycarbyne with itself. The observation that no symmetric coupled product is observed indicates that a bridged intermediate is probably not involved in this reaction.

Formation of $[(dmpe)_2(CO)TaCOZrCp^*_2Cl]$ (4). The formation of **4** in the reaction of $Na[Ta(CO)_2(dmpe)_2]$ (**5**) with $Cp^*_2ZrCl_2$ may be envisioned as a cation-exchange reaction, where the chlorobis(pentamethylcyclopentadienyl)zirconium cation "$Cp^*_2ZrCl^+$" is exchanged for sodium ion. This exchange reaction probably occurs via electrophilic attack at a carbonyl oxygen of **5** by the oxyphilic zirconium complex with subsequent loss of NaCl. Reactivity of this type is similar to that observed upon addition of Me_3SiCl to **5**, which forms a siloxycarbyne. We previously demonstrated that the carbonyl groups in the anion **5** interact extensively with Lewis acids, as evidenced by shifts in the ν_{CO} stretching mode with different counterions.[12,13] The major difference between "$Cp^*_2ZrCl^+$" and other such cations is the highly oxyphilic nature of the zirconium center. This oxyphilicity drives the equilibrium shown in eq 6 to the right.

$$[M{-}C{\equiv}O]M' \rightleftharpoons [M{=}C{=}O{-}M'] \qquad (6)$$

Structures of 3 and 4. An interesting geometric feature observed in the crystal structures of both **3b** and **4** is the nearly linear carbonyl bridge. While in all reported structures of carbonyl-bridged complexes the M–C–O bond angle is within a few degrees of 180°, the M–O–C angle varies from 135.4 (5)° in $[Cp_2Ti(THF)(OC)MoCp(CO)_2]$[19] to 180° in $[Cp^*_2V(OC)V(CO)_5]$,[20] the latter being crys-

Table V. Interatomic Distances (Å) and Angles (deg) for $[(dmpe)_2(CO)TaCOZrCp_2^*Cl]$ (4)[a]

Bond Lengths			
Ta–C(1)	1.932 (5)	Ta–P(4)	2.517 (1)
Ta–C(2)	2.017 (5)	Zr–O(1)	2.010 (3)
Ta–P(1)	2.510 (1)	Zr–Cl	2.466 (1)
Ta–P(2)	2.618 (1)	O(1)–C(1)	1.274 (6)
Ta–P(3)	2.570 (1)	O(2)–C(2)	1.178 (6)
Bond Angles[b]			
C(1)–Ta–C(2)	87.0 (2)	P(3)–Ta–P(2)	96.97 (5)
C(1)–Ta–P(3)	97.9 (1)	P(3)–Ta–P(4)	77.16 (5)
C(1)–Ta–P(1)	94.6 (1)	P(1)–Ta–P(2)	77.03 (4)
C(1)–Ta–P(2)	165.4 (1)	P(1)–Ta–P(4)	172.44 (5)
C(1)–Ta–P(4)	91.0 (1)	P(2)–Ta–P(4)	98.57 (5)
C(2)–Ta–P(3)	170.4 (2)	O(1)–Zr–Cl	94.2 (1)
C(2)–Ta–P(1)	90.8 (2)	C(1)–O(1)–Zr	177.8 (3)
C(2)–Ta–P(2)	81.2 (2)	O(1)–C(1)–Ta	173.4 (3)
C(2)–Ta–P(4)	94.6 (1)	O(2)–C(2)–Ta	178.2 (5)
P(3)–Ta–P(1)	96.96 (5)	O(1)–Zr–Ct(1)	105.1 (3)
Cl–Zr–Ct(1)	103.9 (2)	O(1)–Zr–Ct(2)	104.9 (3)
Cl–Zr–Ct(2)	104.6 (2)	Ce(1)–Zr–Ct(2)	136.5 (5)

Intraligand Geometry

bond or angle type	min	max	mean
$Zr\text{-}C_{ring}$	2.506 (4)	2.601 (5)	2.556
Zr-cent			2.254
P-C	1.793 (7)	1.870 (10)	1.826
(P)C-C(P)	1.37 (1)	1.45 (1)	1.41
$C_{ring}\text{-}C_{ring+1}$	1.394 (7)	1.433 (7)	1.412
$C_{ring}\text{-}C_{exo}$	1.494 (7)	1.526 (7)	1.503
Ta-P-C	108.3 (2)	126.8 (2)	117.8
C-P-C	98.4 (4)	102.2 (4)	99.8
P-C-C	111.5 (4)	118.2 (6)	114.9
$C_{ring}\text{-}Zr\text{-}C_{ring+1}$	31.4 (1)	32.5 (2)	32.1
$Zr\text{-}C_{ring}\text{-}C_{exo}$	118.9 (4)	130.3 (4)	124.9
$C_{exo}\text{-}C_{ring}\text{-}C_{ring+1}$	123.2 (5)	127.0 (5)	125.6

[a] Numbers in parentheses are estimated standard deviations in the last digit(s) given. Standard deviations quoted for the mean values are the average deviations for the individual values. [b] Ct(1) denotes the centroid for the Cp* ring containing C(51)–C(55), Ct(2) denotes the centroid for the Cp* ring containing C(71)–C(75).

Table VI. M–O–C Bond Angles (deg) for Selected Compounds with CO Bridges

compd	angle	ref
$[(CO)_5V(CO)VCp^*_2]$	180	20
$[(CO)_5V(CO)V(THF)_4(OC)V(CO)_5]$	167.7 (9)	25
$[Cp(CO)_2Mo(CO)Zr(Me)Cp_2]$	145.5 (4)	26
$[Cp(CO)_2Mo(CO)TiCp_2]_2$	142.5	19
$[(CO)_3Co(CO)Yb(THF)Cp^*_2]$	163.0 (2)	27
$[(CO)_3Mn(CO)_2YbCp^*_2]_2$	171.6 (9)	28
$[Cp^*(CO)_2Mo(CO)Ti(Me)Cp^*_2]$	144.3 (3)	29
$[Cp(CO)_2Mo(CO)Ti(THF)Cp_2]$	135.4 (5)	19
$[Fe_3(CO)_7(\mu\text{-}CO)_4][YbCp^*_2]_2$	141.9 (4)	30
$[Cp(CO)_2Mo(CO)Zr(\eta^2\text{-}C(O)Me)Cp_2]$	137.4 (3)	31

(16) Vrtis, R. N.; Bott, S. G.; Rardin, R. L.; Lippard, S. J. *Organometallics* **1991**, *10*, 1364.
(17) Mayr, A.; Bastos, C. M. *Progr. Inorg. Chem.*, in press.
(18) Vrtis, R. N.; Liu, S.; Lippard, S. J. Unpublished results.
(19) Merola, J. S.; Campo, K. S.; Gentile, R. A.; Modrick, M. A.; Zentz, S. *Organometallics* **1984**, *3*, 334.
(20) Osborne, J. H.; Rheingold, A. L.; Trogler, W. C. *J. Am. Chem. Soc.* **1985**, *107*, 6292.

tallographically required to have a linear V–O–C–V moiety. A summary of C–O–M bond angles for structurally characterized carbonyl-bridged complexes reported in the literature may be found in Table VI. Examination of these data reveals the angles of 166 (1) and 177.8 (3)° for the M–O–C bond in **3b** and **4**, respectively, to be two of the most nearly linear bridged carbonyl complexes to have been structurally characterized.

Comparison of bond lengths in the bridge with those of known compounds indicates a significant contribution of the canonical form **B** shown in eq 4. The bridging Ta–C distances of 1.96 (2) and 1.935 (5) Å that occur in **3b** and **4**, respectively, are substantially shorter than distances found for compounds having tantalum–carbon single bonds (2.25–2.32 Å) and slightly shorter than those having tantalum–carbon double bonds (2.01–2.03 Å).[21-24] The carbonyl C–O bridge bond distances of 1.27 (2) and 1.269 (6) Å for **3b** and **4**, respectively, are significantly longer than those found in terminal carbonyls and are in fact closer to the value of 1.34 (2) Å occurring in the siloxycarbyne complex [Ta{≡COSi(*i*-Pr)$_3$}(CO)(dmpe)$_2$].[4]

Spectroscopic Properties of 3a and 4. The bridging Ta=C=O–Ta unit in **3a** has an unusually low stretching frequency of 1462 cm^{-1}, which was identified by a ^{13}C labeling experiment. This low value is a further manifestation of the significant oxycarbyne character of this complex, as discussed above. The observed value is nearly identical to that of 1466 cm^{-1} reported for the carbyne ligand in [M{≡COSi(*i*-Pr)$_3$}(CO)(dmpe)$_2$] (M = Ta or Nb).[4] The NMR spectra (^{31}P{^{1}H}, ^{1}H, and ^{13}C{^{1}H}) of **3a** and **4** are all consistent with the geometry observed in the solid state for these complexes being maintained in solution.

Conclusions

Two novel carbonyl-bridged dinuclear compounds have been synthesized and structurally characterized. The first of these complexes, **3a**, is formed by the formal disproportionation of two siloxycarbynes in the presence of sodium chloride. Although **3a** reacts with Me_3SiCl to afford a reductively coupled product, previous work in our laboratory has shown that bridged species of this kind are not likely to be intermediates in the reaction.[5] The heterodimetallic carbonyl-bridged complex **4** has been synthesized by reaction of Na[Ta(CO)$_2$(dmpe)$_2$] with Cp*$_2$ZrCl$_2$. This compound reacts with 2 equiv of Me_3SiCl to yield the reductively coupled product [Ta(Me$_3$SiOCCOSiMe$_3$)(dmpe)$_2$Cl].

Acknowledgment. This work was supported by a grant from the National Science Foundation. We thank Drs. J. D. Protasiewicz and S. Yu for helpful comments on the manuscript.

Registry No. 1, 61916-36-7; **3a**, 137364-76-2; **3b**, 137364-77-3; **4**, 137364-78-4; **5**, 61916-37-8; Me_3SiCl, 75-77-4; *t*-BuMe$_2$SiCl, 18162-48-6; [Ta(Me$_3$SiOCCOSiMe$_3$)(dmpe)$_2$I], 109467-50-7; [Ta(Me$_3$SiOCCOSiMe$_3$)(dmpe)$_2$Cl], 99797-93-0; Cp*$_2$ZrCl$_2$, 54039-38-2.

Supplementary Material Available: Tables S1–S6 reporting non-hydrogen atom thermal parameters and hydrogen atom positional and thermal parameters for [(dmpe)$_2$(CO)TaCOTa(*t*-BuMe$_2$SiOCCOSiMe$_2$-*t*-Bu)(dmpe)$_2$] and [(dmpe)$_2$(CO)TaCOZrCp*$_2$Cl] (9 pages); listings of observed and calculated structure factors for [(dmpe)$_2$(CO)TaCOTa(*t*-BuMe$_2$SiOCCOSiMe$_2$-*t*-Bu)(dmpe)$_2$] and [(dmpe)$_2$(CO)TaCOZrCp*$_2$Cl] (65 pages). Ordering information is given on any current masthead page.

(21) Gibson, V. C.; Grebenik, P. D.; Green, M. L. H. *J. Chem. Soc., Chem. Commun.* **1983**, 1101.
(22) Guggenberger, L. J.; Schrock, R. R. *J. Am. Chem. Soc.* **1975**, *97*, 6578.
(23) Schrock, R. R.; Messerle, L. W.; Wood, C. D.; Guggenberger, L. J. *J. Am. Chem. Soc.* **1978**, *100*, 3793.
(24) Green, M. L. H.; Hare, P. M.; Bandy, J. A. *J. Organomet. Chem.* **1987**, *330*, 61.
(25) Schneider, M.; Weiss, E. *J. Organomet. Chem.* **1976**, *121*, 365.
(26) Longato, B.; Martin, B. D.; Norton, J. R.; Anderson, O. P. *Inorg. Chem.* **1985**, *24*, 1389.
(27) Tilley, T. D.; Andersen, R. A. *J. Chem. Soc., Chem. Commun.* **1981**, 985.
(28) Boncella, J. M.; Andersen, R. A. *Inorg. Chem.* **1984**, *23*, 432.
(29) Hamilton, D. M., Jr.; Willis, W. S.; Stucky, G. D. *J. Am. Chem. Soc.* **1991**, *103*, 4255.
(30) Tilley, T. D.; Andersen, R. A. *J. Am. Chem. Soc.* **1982**, *104*, 1772.
(31) Marsella, J. A.; Huffman, J. C.; Caulton, K. G.; Longato, B.; Norton, J. R. *J. Am. Chem. Soc.* **1982**, *104*, 6360.

Iron–Osmium Bonding in Clusters Containing Ferrocene Fragments

William R. Cullen,* Steven J. Rettig, and Tu-Cai Zheng

Department of Chemistry, University of British Columbia, Vancouver, British Columbia, Canada V6T 1Z1

Received August 13, 1991

Pyrolysis of $Os_3(CO)_{10}(PFcPh_2)_2$ and $Os_3(CO)_{11}(PFc_2Ph)$ affords $Os_3(CO)_8(H)_2[PAr(C_6H_5)(\eta\text{-}C_5H_3)Fe(\eta\text{-}C_5H_4)]$ (Ar = C_6H_5 (**3a**), Fc (**3b**), respectively). $Os_3(CO)_7(H)(PPr^i)[Fe(\eta\text{-}C_5H_4PPr^i_2)(\eta\text{-}C_5H_4)]$ (**4**) is a product of the thermolysis of $Os_3(CO)_{10}[Fe(\eta\text{-}C_5H_4PPr^i_2)_2]$. **3b**: triclinic, space group $P\bar{1}$ (No. 2), a = 13.878 (2) Å, b = 14.145 (3) Å, c = 10.698 (2) Å, α = 104.28 (1)°, β = 110.88 (1)°, γ = 63.91 (1)°. **3a**: monoclinic, space group $P2_1/c$ (No. 14), a = 9.484 (3) Å, b = 18.144 (4) Å, c = 17.421 (3) Å, β = 90.10 (2)°. **4**: monoclinic, space group $P2_1/n$ (No. 14), a = 8.910 (3) Å, b = 22.784 (2) Å, c = 15.416 (2) Å, β = 98.25 (2)°. The complexes are electron precise if the Fe→Os bonds of length 2.830 (1) (**3a**), 2.826 (1) (**3b**), and 2.813 (1) Å (**4**) are included.

There are only a few examples known where the central metal of a metallocene acts as an electron donor to a metal, and most examples are complexes of ferrocene derivatives with the group-8 metals Ni, Pt, and Pd,[1] e.g., complex **1**

0276-7333/92/2311-0277$03.00/0